# UC Irvine
## UC Irvine Previously Published Works

**Title**

Phenomenology of energetic-ion loss from the DIII-D tokamak

**Permalink**

https://escholarship.org/uc/item/15z1q01n

**Journal**

Nuclear Fusion, 50(8)

**ISSN**

0029-5515

**Authors**

Zhu, YB
Heidbrink, WW
Pickering, LD

**Publication Date**

2010-08-01

**DOI**

10.1088/0029-5515/50/8/084024

**Copyright Information**

Peer reviewed

# Phenomenology of energetic-ion loss from the DIII-D tokamak

**Y.B. Zhu, W.W. Heidbrink and L.D. Pickering**

University of California, Irvine, CA 92697, USA

E-mail: yubaoz@uci.edu

**Abstract**
Thin-foil Faraday collectors mounted near the midplane measure energetic-ion loss signals from the DIII-D tokamak. Modulation of the neutral beam sources shows that, under appropriate conditions, prompt losses from every beam line are observed. Prompt losses are usually larger when the plasma current or toroidal field is low. Enhanced losses occur during ion cyclotron heating. Instabilities that produce strong field perturbations at the edge also produce enhanced losses.

PACS numbers: 52.55.Fa, 52.55.Pi, 52.70, 52.35

(Some figures in this article are in colour only in the electronic version)

## 1. Introduction

The loss of energetic ions from magnetic fusion plasma is of both technological and scientific interest. Concentrated losses of fast ions caused by instabilities can damage in-vessel components [1, 2]. In ITER, losses of alpha particles in excess of ~5% are expected to cause damage [3]. Scientifically, loss measurements have verified orbit topology and have identified different mechanisms of transport by instabilities [4].

Historically, several types of fast-ion loss detectors have been employed in tokamaks, including Faraday cups [5], semiconductors [6], scintillators [7], calorimeter and Langmuir probes [8] and infrared cameras [9]. Collimation can be employed to select a particular class of orbit [10] or to analyse pitch-angle and energy distribution [7]. Recent innovative developments include high bandwidth scintillator measurements [11] and collimated probe measurements inside the last closed flux surface [12]. Published papers describe a wide variety of loss mechanisms [4], including prompt losses on the first drift orbit, losses caused by toroidal field ripple and losses caused by various instabilities.

This paper summarizes observations from a pair of thin-foil collectors [13] during several years of operation on the DIII-D tokamak. A few results from these detectors were previously published [13–15] but this is the first comprehensive report on these measurements. Prompt losses that strongly correlate with modulation of a particular beam source are reported for the first time. In addition, examples of losses during a wide variety of different instabilities are given.

The paper begins with a description of the foils (section 2). Examples of modulated prompt losses (section 3), enhanced losses during ion cyclotron heating (ICH, section 4) and losses correlated with magnetohydrodynamics (MHD) instabilities (section 5) are next, followed by a summary and discussion (section 6).

## 2. Apparatus

The two detectors for this study are on opposite edges of the midplane port box that is at a toroidal angle of 60° (figure 1). Each detector consists of a pair of foils: one 'active' foil that is exposed to fast-ion current and one 'blind' foil with nominally identical electrical characteristics that is behind an insulator. The foils are mounted within graphite boxes that have two collimating holes drilled in them (figure 2; see also figure 3 of [13]). The collimating holes point upwards, so only gyrating ions can reach the foil (figure 3); any neutrals or light that might contaminate the signal must be generated within the port box to reach the foil. The collimating holes are relatively large (6.4 mm diameter by 11 mm long), so the pitch-angle and gyro-angle resolution are relatively poor. Calculations with a typical 2 T magnetic field indicate that deuterium ions with energies $\geqslant 10$ keV can reach the foils, implying that the detectors are sensitive to both the beam ions and the tail of the thermal-ion distribution in hot plasmas. When the toroidal field is reversed from its normal clockwise (CW) direction, no ion current should reach the detector and, indeed, negligible signals are measured when the field is counter-clockwise (CCW). In the horizontal direction, the holes are tilted at an angle to specify the toroidal velocity vector. The collimating holes are recessed 1.9 cm radially from the graphite tiles that armour the outer wall of the DIII-D vessel. The port box is 35 cm wide.
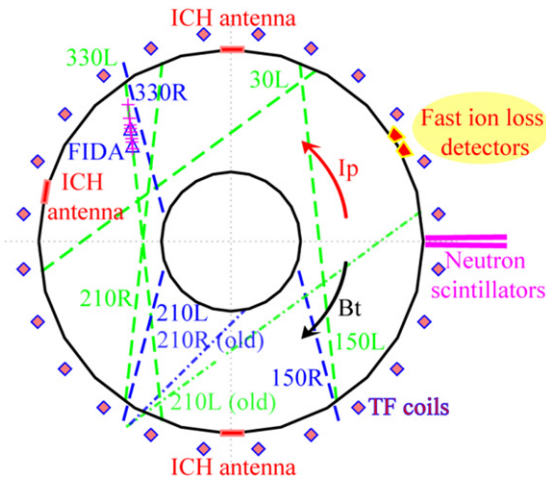
**Figure 1.** Plan view of the DIII-D vessel. The fast-ion loss detectors are located in the 60° port. Neutral beam footprint centre lines (dashed) and the toroidal locations of the toroidal field coils (diamonds), ICH antennas (small red rectangles), neutron scintillators (long magenta rectangles) and vertical FIDA sightlines are also shown. The beam sources are identified by the toroidal angle of the vessel flange. The normal directions for the plasma current and toroidal field are CCW and CW, respectively. (Colour version online.)
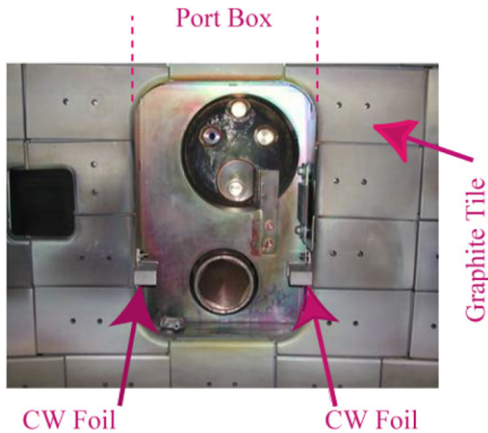


**Figure 2.** Photograph of the midplane port at 60°. The foil detectors are located in small graphite boxes at the left and right edges of the port. The port is surrounded by the graphite tiles that constitute the first wall.

Hence, any orbit that reaches the foil must move outwards at least 1.9 cm radially when it moves toroidally 35 cm, i.e. $\Delta R/(R|\Delta\phi|) \geqslant 0.05$, in order to avoid being 'scraped off' by a graphite shield tile. For most fast-ion orbits, this is the strongest constraint on access to the foil. Unlike some tokamaks, the DIII-D outer wall has very few protrusions, so the main obstacle to incoming orbits is the graphite tiles that surround the port box.

Toroidal field ripple is relatively weak in DIII-D (typically 0.4% at the last closed flux surface) and is ignored in our analysis. The tokamak has 24 toroidal field coils that are outside the field-shaping coils, so the toroidal field ripple is $\leqslant$1% even near the foils.

Apart from special tests, the foils are unbiased. (Tests with the foils biased indicate that secondary electron production has a small impact on the measured currents.) The collected
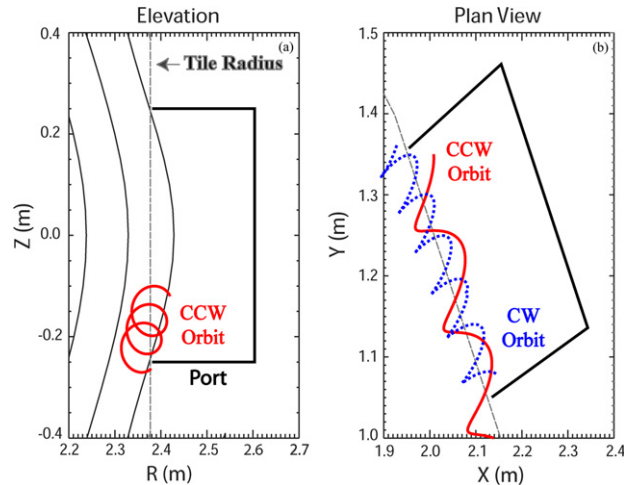


**Figure 3.** Side and top views of the port box that houses the two foil detectors and projections of two representative beam-ion orbits that reach the foils. (*a*) The foils are 12 cm below the horizontal midplane. Orbits enter the collimating holes from above. (In this projection, the CCW and CW orbits are similar, so only the CCW orbit is shown for clarity.) (*b*) The accepted orbits move out radially as they traverse toroidally to a foil at the opposite edge of the port box. The CCW orbit (solid red spiral) with $dR/d\phi < 0$ is calculated for an equilibrium with $I_p = 1.2$ MA in the CCW direction and $B_T = 1.6$ T; the CW orbit (blue dotted spiral) is calculated for an equilibrium with $I_p = 1.6$ MA in the CW direction and $B_T = 2.1$ T. (Colour version online.)

currents are carried by coaxial cables through a vacuum feedthrough to a commercial transimpedance amplifier with an input impedance of 100 Ω. The output of the amplifier passes through an optical break (~100 kHz bandwidth) and is digitized (typically at 500 kHz). Typical signal levels correspond to current densities of O(1) A m$^{-2}$. To minimize common-mode interference, the signals reported in this paper are usually difference signals from an active/blind foil pair with the dc offset subtracted. In the case of high-frequency signals, the oscillation amplitude on the active foil is O(100) times larger than the oscillation amplitude on the blind foil.

The DIII-D tokamak is equipped with seven neutral beam injection (NBI) sources (figure 1) that are identified by the toroidal angle of the beam port. (Throughout the paper, the toroidal angle $\phi$ increases in the CW direction.) Prior to 2006, all seven sources injected ions in the CCW direction. Between the 2005 and 2006 experimental campaigns, the beam line at 210° was reoriented to inject in the CW direction. (The data in this paper span from 2005 through February 2009.) Typically, the beams inject deuterium neutrals at an injection energy $\leqslant$ 81 keV. The sources inject at two tangency radii: near-perpendicular (0.76 m) and near-tangential (1.15 m). The usual directions for the plasma current $I_p$ and the toroidal field $B_T$ are CCW and CW, respectively.

DIII-D has fast-wave antennas located at toroidal angles of 0°, 180° and 285°. The 285° antenna is connected to a 60 MHz transmitter. The 0° and 180° antennas launched waves at 83–120 MHz during the campaigns included in this paper. Coupled powers of $\geqslant$1 MW per antenna are typical.

In addition to the foils, DIII-D has several other fast-ion diagnostics, including neutron scintillators [16] and vertically viewing fast-ion D-alpha (FIDA) spectrometers [17].

2
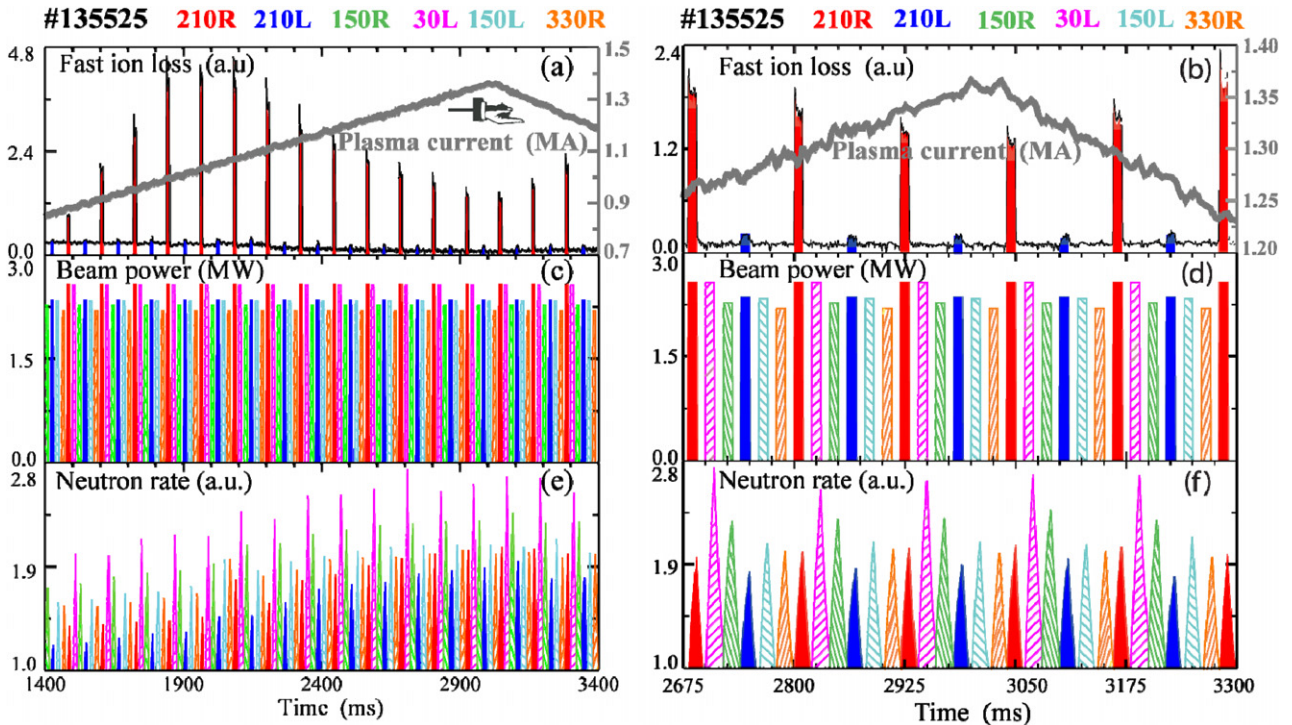
**Figure 4.** Time evolution on two different time bases of (*a*) and (*b*) CCW foil current and plasma current, (*c*) and (*d*) neutral beam power, (*e*) and (*f*) neutron rate in a discharge with modulated beam injection by six different sources. (Overall, the beams inject 50% of the time.) The signals are colour-coded to indicate which beam produced the signal. The toroidal field (2.0 T), outer gap (6.4 cm) and electron density ($\bar{n}_{\rm e} = 3.4 \times 10^{19}\,{\rm m}^{-3}$) are nearly constant during this portion of the discharge. 210R and 210L inject in the CW direction; all other sources inject CCW. (Colour version online.)

## 3. Prompt losses

During normal operation at DIII-D, the various NBI sources are often modulated for diagnostic purposes or for feedback control of a particular quantity (such as beta or toroidal rotation). Direct losses correlated with modulation of a particular source are often observed. Figure 4 shows an example from a discharge devoted to the study of these prompt losses. In this discharge, six different sources inject 10 ms beam blips; the beam timing is arranged so that there are 10 ms gaps between every beam pulse (figures 4(*c*) and (*d*)). As expected, the neutron rate, which is proportional to the total number of confined fast ions, rises during each beam pulse and decays between pulses (figures 4(*e*) and (*f*)). In contrast, the CCW foil detects large losses only when the near-tangential 210° source injects (figures 4(*a*) and (*b*)). Small increases correlate with injection of the near-perpendicular 210° source, while the other sources have no detectable effect. Figure 4 also illustrates the strong dependence on plasma current of the detected prompt losses. In this case, the losses associated with the 210° near-tangential source are greatest when the plasma current is about 1.0 MA.

Figure 5 shows a more complicated example. In this discharge, the foil current increases whenever the near-tangential 330° source injects into the plasma and small increases are noticeable when the near-tangential 210° and 30° sources inject.

For the proper conditions, any source can produce this sort of response on a foil detector. On occasion, every source has produced a modulated prompt response on one of the foil

detectors, including the sources at 210° both before and after their injection angle was rotated. Generally speaking, the phenomenon is most common in low current and low toroidal field discharges. In the sequence of discharges illustrated in figure 6, the prompt losses from the near-tangential counter-current beam at 210° are largest in the lowest current discharge. Figure 7 shows the signal associated with modulation of the near-tangential 210° source in a sequence of discharges with different values of toroidal field. The signals are largest for the smallest toroidal field. Because the drift orbits and gyro-radii are larger at lower current and toroidal field, respectively, these general trends are expected for prompt losses. However, it is *not* true that the measured prompt losses from a particular source are invariably maximized for low fields. For example, for the dedicated discharges that include figure 4, the largest losses occur at about 1.0 MA.

Modelling with a Lorentz orbit code verifies that prompt modulated losses are observed when injected neutrals ionize on orbits that eventually collide with the foils. Figure 8 shows an example. To model this phenomenon, a discharge with prompt losses from a particular source is selected. The magnetic fields are obtained by solving the Grad–Shafranov equation with the equilibrium fitting code EFIT [18]. The collimating apertures at the foils define 'initial' conditions that are used to trace orbits backwards in time in the equilibrium fields (neglecting Coulomb collisions, since orbital timescales are orders of magnitude shorter than collisional timescales). When the orbit intersects the footprint of the neutral beam source that produces the modulated signal, the velocity vector is checked to see if it is consistent with the possible injection velocities
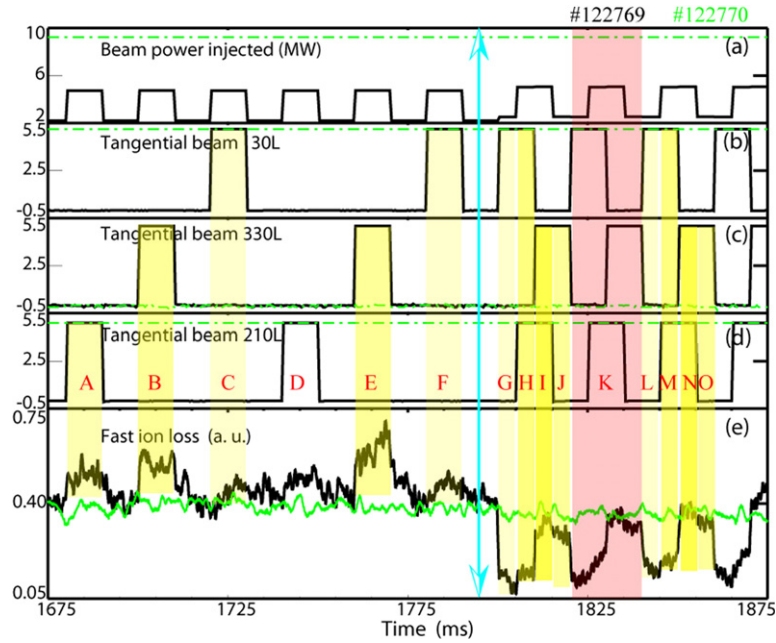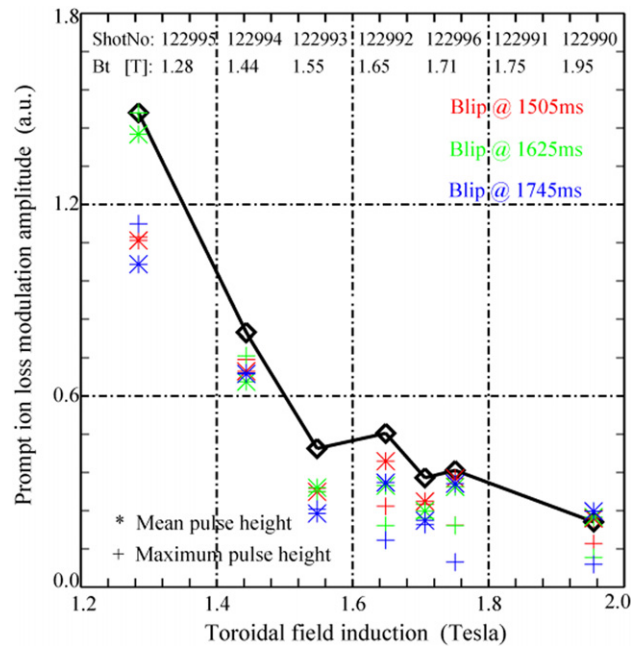
**Figure 5.** Single and compound beam-modulated prompt loss. Green lines are from a neighbouring non-modulated shot with twice the injected power. (*a*) Total injected beam power, (*b*) (*c*) (*d*) the near-tangential beams at 30°, 330° and 210° (all injecting in the CCW direction), (*e*) CCW foil signal. Coloured shadows highlight the correlation between fast-ion loss and the injected beam blips. A–F and G–O show the single and compound modulated prompt beam-ion loss pattern, respectively. $I_p = 1.0$ MA; $B_T = 2.0$ T; $\bar{n}_e = 2.3 \times 10^{19}$ m$^{-3}$. (Colour version online.)
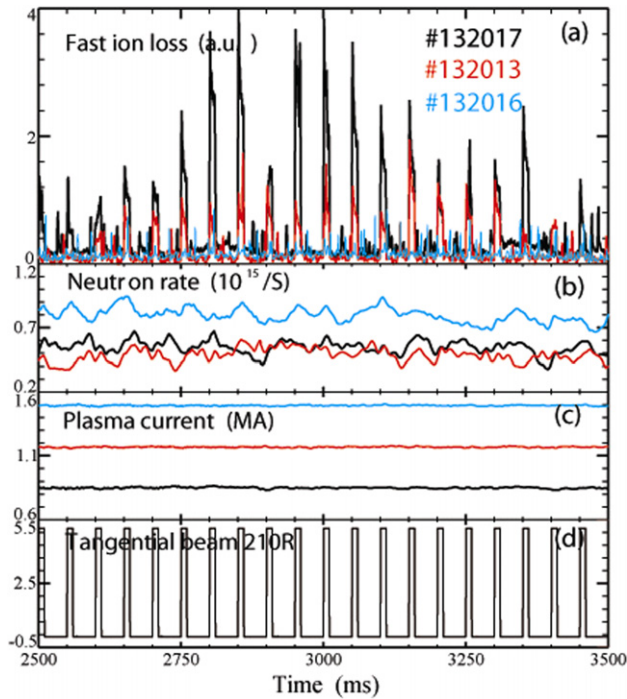


**Figure 6.** Time evolution of the (*a*) CCW foil signal, (*b*) neutron rate, (*c*) plasma current and (*d*) timing of the near-tangential 210° source injecting in the counter-current (CW) direction in a set of discharges with $B_T = 2.1$ T and $\bar{n}_e \cong (4-6) \times 10^{19}$ m$^{-3}$.



**Figure 7.** Prompt loss modulation amplitude for the near-tangential 210° source versus $B_T$. Signal basements just in front of the pulses are subtracted from the maximum pulse height, while no basement is subtracted from the mean pulse height. The heavy line goes through the uncorrected maximum pulse height.

of injected neutrals. Orbits that satisfy the requisite conditions occur near the edge of the plasma at both large and small major radii.

Conceptually, fast-ion orbits constitute a trajectory in phase space. Detection of prompt losses from a particular source occurs only when the phase space populated by beam ionization 'connects' to the phase space measured by the foil. Connection of these relatively small phase space volumes requires precise matching of both the radial and the toroidal location of the ionization event. This explains why it is rare for more than one source to produce appreciable modulated
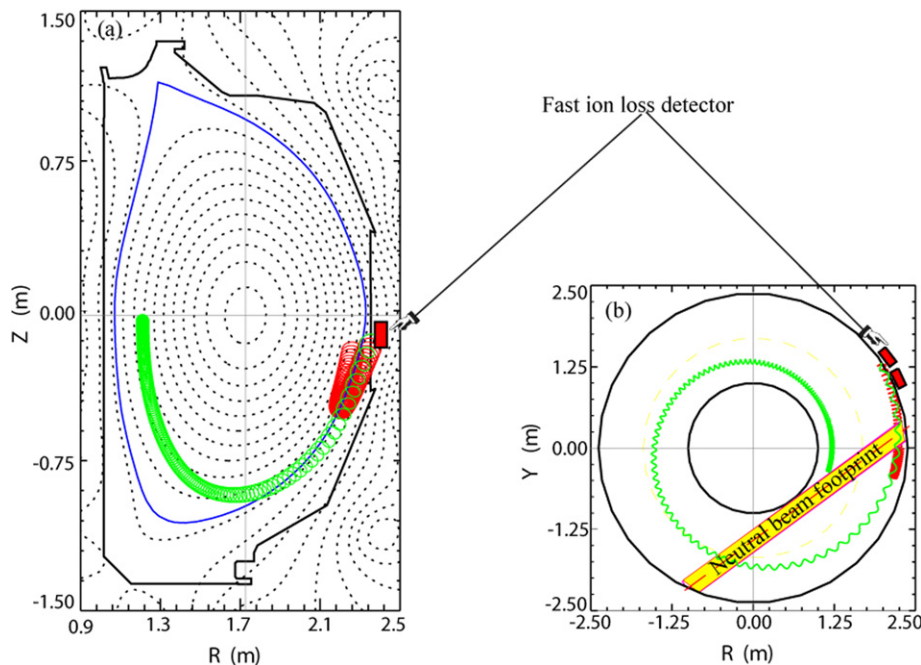
**Figure 8.** Typical prompt loss ion trajectory from the 210° near-tangential neutral beam to the CCW fast-ion loss detector as calculated by a Lorentz orbit code for a DIII-D discharge with strong modulated prompt beam-ion loss. (*a*) Poloidal view, (*b*) toroidal view. The long green spiral trajectory indicates that escaping beam ions can reach the foil from the inner part of the beam footprint. The short red spiral trajectory shows that neutrals that ionize near the plasma boundary can shoot directly into the detector. $I_p = 1.0$ MA; $B_T = 1.27$ T.

losses at a particular time in the discharge. It also explains why the signals are maximized for particular values of plasma current and field. Modulated prompt losses are observed at both high and low plasma density, which is consistent with calculations that show that orbits from either large major radius or small major radius can connect the foil apertures to the beam footprint. Many of the discharges with the largest modulation amplitude are low density discharges. In these discharges, beam attenuation is weak, so significant numbers of neutrals ionize at small major radius or even after returning to large major radius, as in figure 8.

Only one of the two foil detectors measures appreciable signals at any one time. Ions must drift toroidally in the direction of the plasma current to be detected (figure 3). When $I_p$ is in the usual CCW direction, signals are observed on the CCW foil mounted on the left side of the port box ($\mathrm{d}R/\mathrm{d}\phi < 0$ as the ion approaches the foil). When the sign of the plasma current is reversed, signals are measured on the opposite foil. Interestingly, the beam that produces the modulated signal can inject in either the co- or counter-current direction. Since trapped ions reverse the direction of their toroidal drift, the initial sign of $\dot\phi$ is less important than the sign of $\mathrm{d}R/\mathrm{d}\phi$ at the port box.

## 4. Increased losses during ion cyclotron heating

Enhanced losses are often observed during fast-wave at frequencies between 60 and 120 MHz. Figure 9 shows an example from data acquired during the experiments described in [19, 20]. In these experiments, the fast waves damp on deuterium beam ions at central resonances between the fourth and the eighth cyclotron harmonics; in addition to the primary central resonance, there are additional resonance layers near

the plasma edge. Either the 116 MHz antenna at 180° or the 60 MHz antenna at 285° can increase the fast-ion loss. As usual, appreciable signals are only observed on the foil that accepts ions travelling in the same direction as the plasma current (CCW in this case). The response to the ICH power is rapid (figure 10). Conditional averaging of many pulses shows that, when the ICH turns on, the foil signal rises in 1.0 ms to a steady value then, when the ICH turns off, falls in 1.0 ms to its original value. A rapid response is observed for both antennas (figure 9).

The magnitude of the enhanced losses usually increases with ICH power (figure 11). As with prompt losses, ICH-induced losses tend to increase with decreasing toroidal field (figure 12). Factor-of-two changes without any obvious change in plasma parameters are sometimes observed. As illustrated in figure 9, there is no obvious dependence of the ICH-induced losses on the angle of beam injection.

## 5. Losses during MHD instabilities

Perturbations of the magnetic field associated with instabilities often produce enhanced fast-ion losses. Although there is some correlation of enhanced signals with core MHD activity, the strongest correlation is with instabilities that cause large edge perturbations, such as edge localized modes (ELMs) or the edge harmonic oscillation (EHO). Often, the largest losses occur in discharges with both core and edge instabilities. This section shows representative examples. In general, the relationship between the mode amplitudes and the measured foil currents is too complex to be described by a simple scaling relationship.

Figure 13 shows a discharge that is dominated by an $m = 3$, $n = 2$ neoclassical tearing mode (NTM) [21] initially
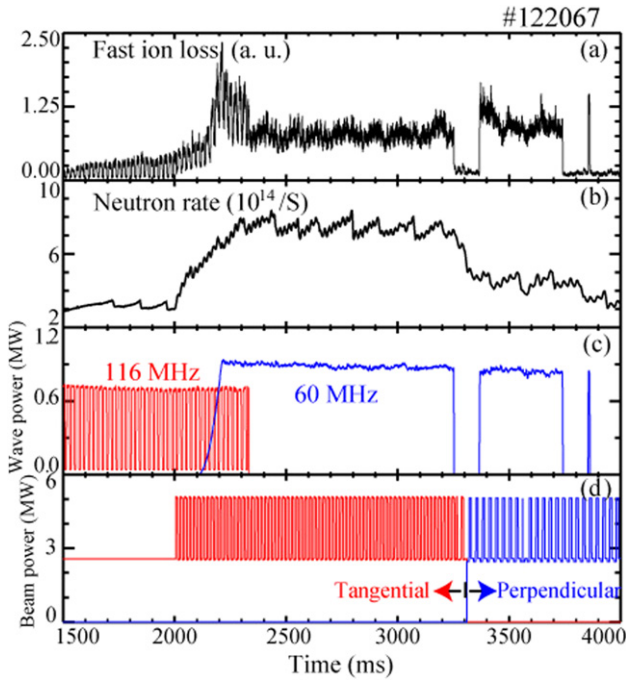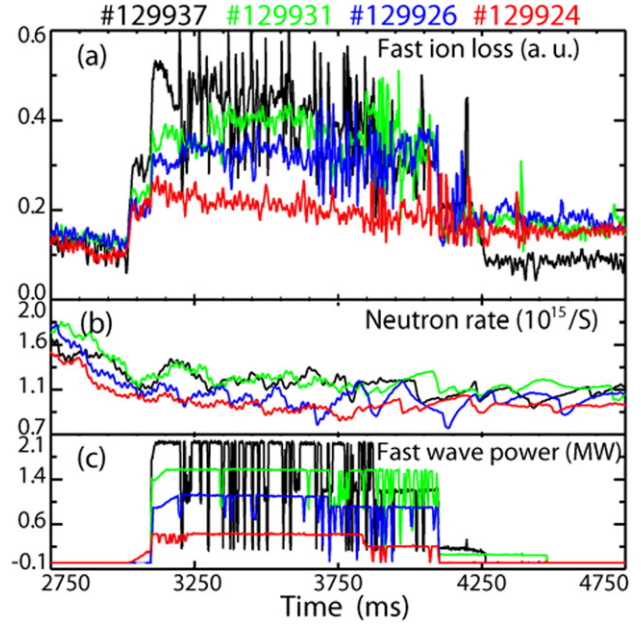
**Figure 9.** Time evolution of the (*a*) CCW foil signal, (*b*) neutron rate, (*c*) coupled fast-wave power from the 116 MHz antenna at 180° and coupled power from the 60 MHz antenna at 285° and (*d*) injected beam power. The neutral beam sources switch from near-tangential to near-perpendicular at 3300 ms. $I_p = 1.0$ MA; $B_T = 1.87$ T; $\bar{n}_e \cong 2.0 \times 10^{19}$ m$^{-3}$.
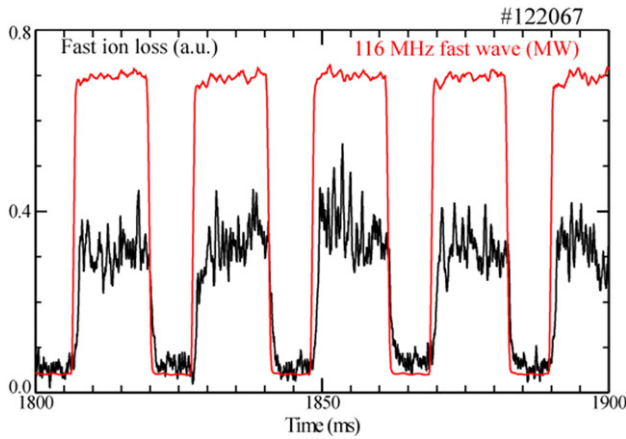


**Figure 10.** Details of the foil and ICH power signals shown in figure 9.

and by $n = 1$ fishbone [22] bursts later in the discharge (after 3000 ms). Large bursts on the foil currents occur when the internal MHD combines with ELM activity. Figure 14 details one of these bursts and illustrates many typical features of the data.

- There is generally a delay between ELM onset (as indicated by the initial rise of the D$_\alpha$ light) and the foil current signal.
- In this discharge, a burst in the loss signal occurs at virtually every burst of D$_\alpha$ light.
- The detailed time evolution of the loss signal does not follow the evolution of the D$_\alpha$ light. Rapid oscillations



**Figure 11.** Time evolution of the (*a*) CCW foil signal, (*b*) neutron rate and (*c*) 90 MHz fast-wave power in a series of discharges with $B_T = 1.94$ T, $I_p = 1.56$ MA, total injected beam power $P_{NBI} = 8$ MW and $\bar{n}_e \cong (4\text{–}5) \times 10^{19}$ m$^{-3}$.
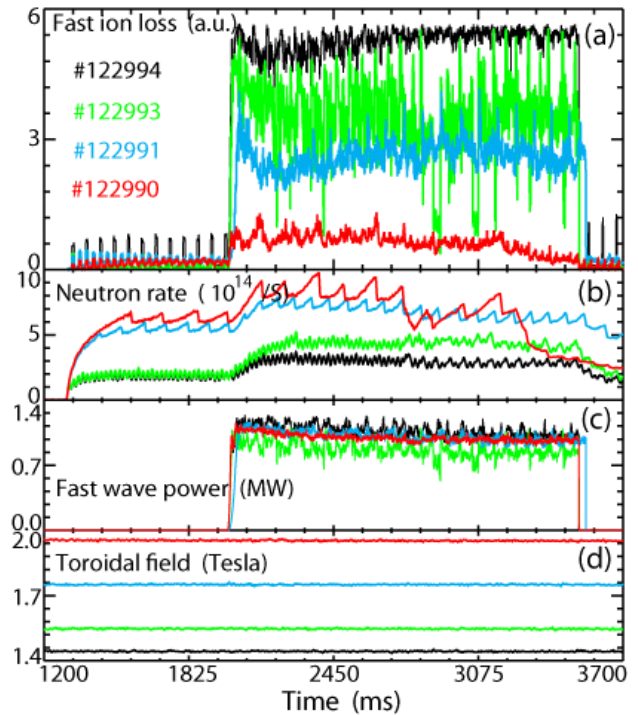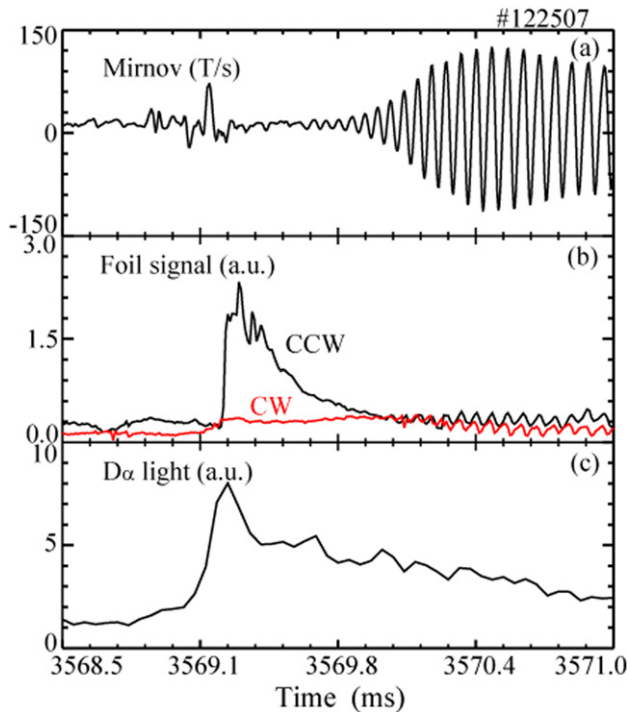


**Figure 12.** Time evolution of the (*a*) CCW foil signal, (*b*) neutron rate, (*c*) coupled 60 MHz fast-wave power and (*d*) toroidal field in a series of discharges with beam power between 1.2 and 2.5 MW and $\bar{n}_e = 1.9 \times 10^{19}$ m$^{-3}$. (Note the fast-ion loss signal is clipped by the electronics in discharge #122994.)

(often much larger than the ones at 3569.3 ms in figure 14) are common. A likely explanation for this variability is that the toroidal asymmetries of the ELM cause fast-ion loss at different toroidal locations at different times.
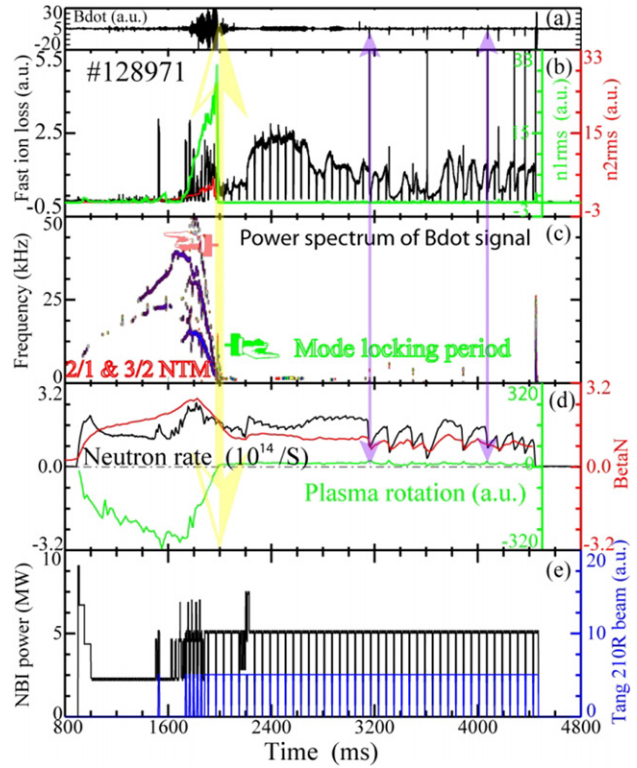
6
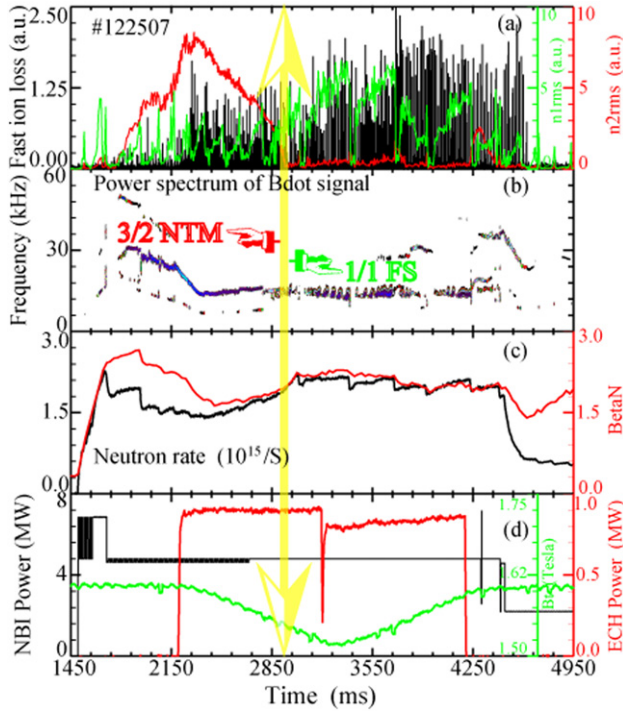
**Figure 13.** Discharge with NTM and fishbone activity. (*a*) CCW fast-ion loss signal (black), $n = 1$ and $n = 2$ mode amplitude are shown in green and red lines, respectively, (*b*) autopower spectrum of midplane $\dot{B}$ signal, (*c*) neutron rate and $\beta_N$ (beta normalized by $I_p/aB_T$), (*d*) injected NBI power, ECH power and toroidal field. (Colour version online.)



**Figure 15.** Sustainment of significant fast-ion loss by a locked mode. (*a*) midplane $\dot{B}$ evolution, (*b*) CCW foil signal (black), $n = 1$ and $n = 2$ mode amplitude are shown in green and red lines, respectively, (*c*) autopower spectrum of midplane $\dot{B}$ signal, (*d*) neutron rate, normalized and plasma rotation speed and (*e*) injected neutral beam power and the near-tangential 210° beam timing. (Colour version online.)



**Figure 14.** Time evolution of the (*a*) midplane $\dot{B}$ signal, (*b*) foil currents and (*c*) $D_\alpha$ light during an ELM in the discharge shown in figure 13.

- The temporal correlation is usually stronger with edge modes than with core modes like a fishbone.

Nevertheless, there are many discharges where ELMs do not cause significant increases in foil current. Apparently, the combination of core and edge modes acts synergistically to enhance the fast-ion losses, with the largest losses occurring when a core instability transports fast ions to the portion of phase space that is depopulated by an edge instability [23].

Large radial magnetic fields can cause large losses. Figure 15 shows a discharge with a locked mode. Early in the discharge, the tearing mode rotates and is detected on a Mirnov coil. After the mode locks at 1980 ms, the foil current increases in amplitude.

The radial component of the magnetic field often correlates better with the observed losses than other measures of magnetic activity. Figure 16 shows a set of three discharges with both Alfvén eigenmode (AE) and low-frequency MHD modes. The strongest correlation of the foil current signal is with the amplitude of the radial magnetic field measured by a midplane probe (figure 16(*b*)).

Enhanced losses often occur in discharges with beam-driven AE [24] activity. Figure 17 shows an example from a strongly driven discharge with both toroidicity-induced Alfvén eigenmode (TAE) and reversed-shear Alfvén eigenmode (RSAE) activity. The losses correlate more strongly with the low-frequency radial magnetic field (figure 17(*b*)) than with the
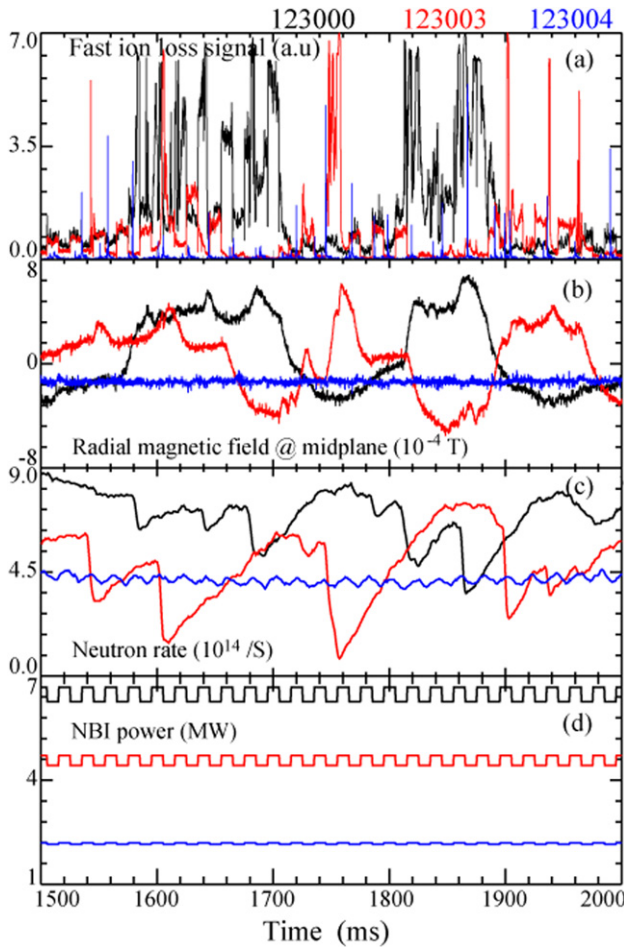
**Figure 16.** Correlation with radial magnetic field. (*a*) CCW foil signal, (*b*) radial magnetic field at the midplane at 199°, (*c*) neutron rate and (*d*) injected beam power.



**Figure 17.** Discharge with AEs. (*a*) Autopower spectrum of CCW foil signal, (*b*) CCW foil signal and radial magnetic field, (*c*) neutron rate and injected NBI power, (*d*) mode amplitude evolution averaged with ±10 kHz bandwidth along spectrum peaks above and below 50 kHz, (*e*) autopower spectrum of midplane $\dot{B}$ signal and nominal TAE frequency (red). (Colour version online.)
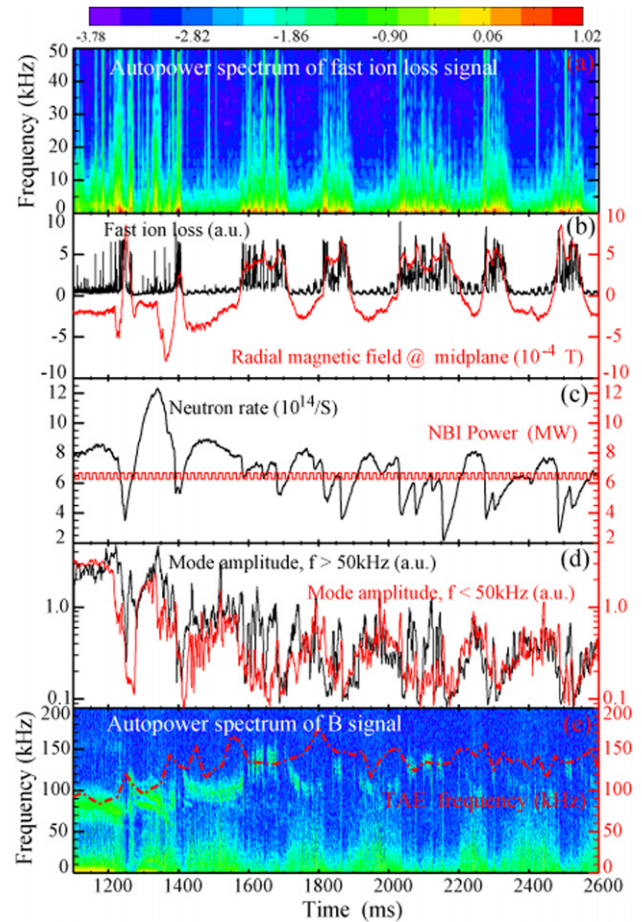
high-frequency AE activity (figure 17(*d*)). Another example of losses during AE activity appears in figure 15 of [15]. As in the case shown here, large losses occur during a phase of the discharge with strong Alfvén activity but the temporal correlation with the core mode amplitude is weak.

Enhanced losses are often observed during quiescent H-modes [14]. The losses often correlate with the incidence of the EHO (figure 18) [26]. Fourier analysis of the foil current shows a broadband of oscillations up to 100 kHz. This phenomenon is common during counter-injected quiescent H-mode operation. The broadband losses usually correlate with EHO activity but not always.

## 6. Summary and discussion

The foil collectors are a simple and reliable fast-ion loss diagnostic. Interesting signals are obtained on virtually every beam-heated discharge. Prompt losses associated with modulation of a particular beam source are common. These losses are most evident in discharges with low toroidal or poloidal fields but have been detected in a wide variety of conditions.

Enhanced losses are observed during fast-wave heating. These losses are usually largest at low toroidal field and at

high ICH power. Enhanced losses are also associated with ELMs, with radial magnetic fields during mode locking and with broadband MHD. The signals often contain frequency components up to 100 kHz.

The prompt losses are readily explained by the combination of neutral beam deposition geometry and collisionless orbits in the equilibrium field. The other phenomena reported in this paper are more difficult to model. Presumably, the enhanced losses during ICH are caused by ion cyclotron acceleration of beam ions near the plasma edge. Proper modelling of these losses requires knowledge of the edge wave fields, including toroidal variations. For the losses induced by instabilities, interpretation is complicated by the fact that the loss foils only observe a small portion of phase space and often involve the synergistic effect of both core and edge instabilities. Nevertheless, it would be useful to predict the foil currents in modelling of the effect of wave fields on the fast-ion orbits, as was done in [27, 28] (for example). It would also be useful to measure the wave fields at the location of the foils, as in recent work by Nagaoka *et al* [12].
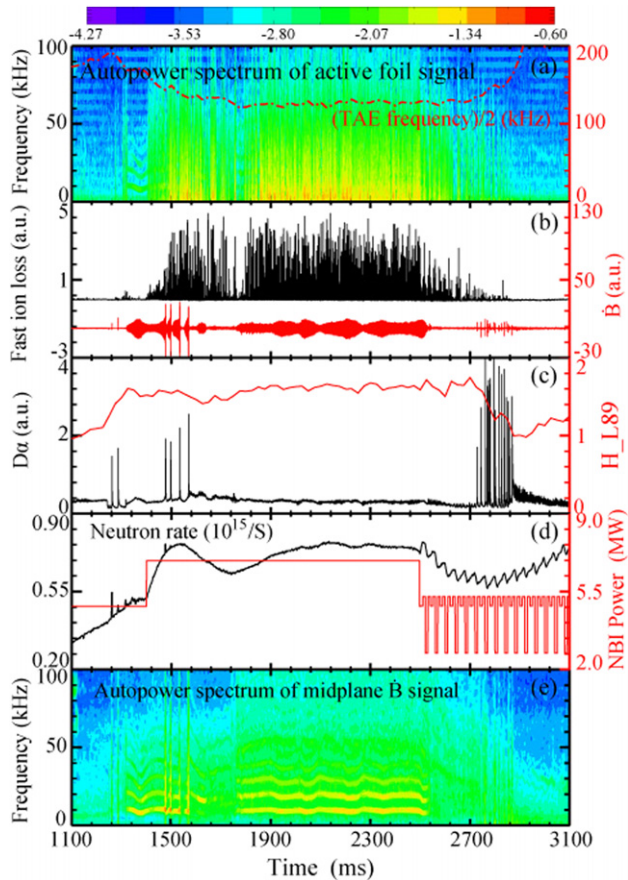
**Figure 18.** Fast-ion loss bursting via EHO during a quiescent
H-mode. (*a*) Autopower spectrum of CW foil signal and half of the
nominal TAE frequency, (*b*) CW foil signal and midplane $\dot{B}$ signal,
(*c*) divertor $D_\alpha$ signal and normalized energy confinement time
(H-L89 factor) [25], (*d*) neutron rate and NBI power, (*e*) autopower
spectrum of midplane $\dot{B}$ signal.

## Acknowledgments

## References

[1] Duong H.H. *et al* 1993 *Nucl. Fusion* **33** 749
[2] White R.B. *et al* 1995 *Phys. Plasmas* **2** 2871
[3] ITER Physics Expert Group on Energetic Particles,
    Heating and Current Drive *et al* 1999 *Nucl. Fusion*
    **39** 2471
[4] Heidbrink W.W. and Sadler G.J. 1994 *Nucl. Fusion*
    **34** 535
[5] Tuszewski M. and Roubin J.P. 1988 *Nucl. Fusion*
    **28** 499
[6] Chrien R.E. *et al* 1981 *Phys. Rev. Lett.* **46** 535
[7] Zweben S.J. 1989 *Nucl. Fusion* **29** 825
[8] Manos D.M. *et al* 1982 *J. Nucl. Mater.* **111–112** 130
[9] Tobita K. *et al* 1995 *Rev. Sci. Instrum.* **66** 594
[10] Heidbrink W.W. and Strachan J.D. 1985 *Rev. Sci.
    Instrum.* **56** 501
[11] García-Muñoz M. *et al* 2008 *Phys. Rev. Lett.*
    **100** 055005
[12] Nagaoka K. *et al* 2008 *Phys. Rev. Lett.* **100** 065005
[13] Cecil F.E. *et al* 2003 *Rev. Sci. Instrum.* **74** 1747
[14] West W.P. *et al* 2005 *J. Nucl. Mater.* **337–339** 420
[15] Heidbrink W.W. *et al* 2008 *Nucl. Fusion* **48** 084001
[16] Heidbrink W.W. *et al* 1997 *Rev. Sci. Instrum.* **68** 536
[17] Luo Y. *et al* 2007 *Rev. Sci. Instrum.* **78** 033505
[18] Lao L.L. *et al* 1985 *Nucl. Fusion* **25** 1611
[19] Pinsker R.I. *et al* 2006 *Nucl. Fusion* **46** S416
[20] Heidbrink W.W. *et al* 2007 *Plasma Phys. Control. Fusion*
    **49** 1457
[21] Chang Z. *et al* 1995 *Phys. Rev. Lett.* **74** 4663
[22] McGuire K. *et al* 1983 *Phys. Rev. Lett.* **50** 891
[23] Gobbin M. *et al* 2009 *Nucl. Fusion* **49** 095021.
[24] Heidbrink W.W. 2008 *Phys. Plasmas* **15** 055501
[25] Yushmanov P.N. *et al* 1990 *Nucl. Fusion* **30** 1999
[26] Burrell K.H. *et al* 2001 *Phys. Plasmas* **8** 2153
[27] Zweben S.J. *et al* 1999 *Nucl. Fusion* **39** 1097
[28] García-Muñoz M. *et al* 2007 *Nucl. Fusion* **47** L10